TiMEpy: A Python Package for Analyzing Tidal Modulation of Fast and Slow Earthquakes

Weifan Lu[1*]

1 ISTerre, Université Grenoble Alpes, CNRS, Université Savoie Mont Blanc, IRD, Université Gustave Eiffel, Grenoble, France

[*]Corresponding author: lu.weifan@univ-grenoble-alpes.fr

Author ORCIDs

Weifan Lu: 0000-0003-4553-8886

Author contributions

Conceptualization: W. Lu
Data Curation: W. Lu
Formal Analysis: W. Lu
Funding Acquisition: W. Lu
Investigation: W. Lu
Methodology: W. Lu
Project Administration: W. Lu
Resources: W. Lu
Software: W. Lu
Supervision: W. Lu
Validation: W. Lu
Visualization: W. Lu
Writing – original draft: W. Lu
Writing – review & editing: W. Lu

Abstract

Due to interactions between the solid Earth and tidal forces, the crust experiences continuous stress perturbations. Understanding how earthquakes respond to tidal stresses provides unique insights into the mechanisms governing earthquake nucleation. Here, we present TiMEpy, an open-source Python package designed to detect tidal modulation in both fast and slow earthquakes. TiMEpy includes fundamental tools for earthquake declustering, converting tidal strain to stress, and correlating earthquakes with tidal stress by extracting phase and level information. Based on these phase and level data, the package offers three methods to evaluate the strength of tidal modulation. TiMEpy can be applied not only to time-series analyses preceding large earthquakes, but also to regional or grid-based investigations of earthquake–tidal correlations. To validate its performance, we applied TiMEpy to the Ridgecrest earthquakes in California and tectonic tremors in Taiwan, demonstrating its stability and reliability. Overall, TiMEpy provides an effective framework for examining earthquake–tidal interactions, offering researchers and practitioners a powerful tool for advancing our understanding of earthquake physics.

1. Introduction

Earthquakes, the sudden release of energy in the Earth's crust, are influenced by a complex interplay of factors, including tectonic stresses, fault properties, and external forces (Ader et al., 2012). Among these external forces, tidal stresses induced by the gravitational pull of the moon and sun have long been hypothesized to modulate earthquake activity. The relationship between tidal forces and earthquake triggering has been a topic of debate and investigation for over a century. While some studies have suggested a correlation between tidal stresses and earthquake occurrence (e.g. Beaucé et al., 2023; Cochran et al., 2004; Cotton, 1922; Tanaka, 2012), others have found little to no evidence of such a connection (e.g. Heaton, 1982; Shudde & Barr, 1977; Vidale et al., 1998; Wang & Shearer, 2015). This ongoing debate stems from the complexity of earthquake mechanics, the subtlety of tidal influences, and the difficulty of statistically isolating tidal effects from other factors controlling earthquake timing. Compared with fast earthquakes, slow earthquakes, such as low-frequency earthquakes (Shelly et al., 2007) and tectonic tremors (e.g. Lu & Ide, 2026; Obara, 2002), have shown an exponential relationship between tremor rates and tidal stress, although the degree of sensitivity varies by region (e.g. Beeler et al., 2013; Houston, 2015; Ide et al., 2015; Shelly et al., 2026; Thomas et al., 2012; Xue et al., 2025; Yabe et al., 2015). Hence, a more systematic approach is needed to evaluate whether and how tides influence earthquake triggering across diverse tectonic settings.

Nevertheless, several factors may obscure or weaken any observable correlation between earthquakes and tides. One such factor is the limited number of events in some datasets, which reduces statistical power. Another issue is the lack of earthquake declustering, which can introduce bias when evaluating the correlation between tidal stresses and earthquake occurrence. Furthermore, many existing methods rely on a single analytical approach, such as Schuster’s test, which considers only the tidal phase while overlooking the level of tidal stresses. Recent advances in earthquake detection technology have led to the creation of numerous long-duration, high-quality catalogs, making it possible to conduct more systematic investigations of earthquake–tidal correlations (Beaucé et al., 2023; Guo et al., 2026; Lu, Xue, et al., 2025; Ross, Trugman, et al., 2019; Sirorattanakul & Avouac, 2026).

In response to these challenges, we present a comprehensive Python package designed to systematically investigate the tidal modulation of earthquakes. Our approach incorporates both tidal phase and level information, providing a more complete assessment of how tides may influence earthquake triggering. By offering a more robust and flexible framework for analyzing tidal effects, this package aims to improve our understanding of the relationship between tidal stresses and seismic activity, ultimately contributing to better seismic hazard assessment.

2. Overview of TiMEpy

The workflow of TiMEpy, illustrated in **Figure 1**, comprises two interconnected modules: Preprocessing and Analysis. The Preprocessing module begins by refining seismic catalogs using declustering methods to isolate independent mainshocks from clustered aftershocks and foreshocks. Concurrently, tidal strain data derived from lunar and solar gravitational forces are converted into tidal stress tensors using a strain-to-stress procedure that accounts for regional crustal elasticity and heterogeneity, ensuring accurate stress perturbation estimates at fault.

Within the Analysis module, the declustered earthquake catalog is integrated with tidal stress data to extract the tidal phase and level corresponding to each earthquake's timing. These parameters are then scrutinized using methods such as Schuster’s test and tidal phase-level analysis to identify potential tidal triggering thresholds. To accommodate spatial and temporal variability, the framework employs three partitioning strategies: whole-region aggregation, grid-based spatial segmentation to capture localized modulation effects, and pre-seismic correlation analysis to explore tidal stress patterns preceding earthquake sequences. Additionally, b-value measurements are incorporated to further assess how it evolves over time.

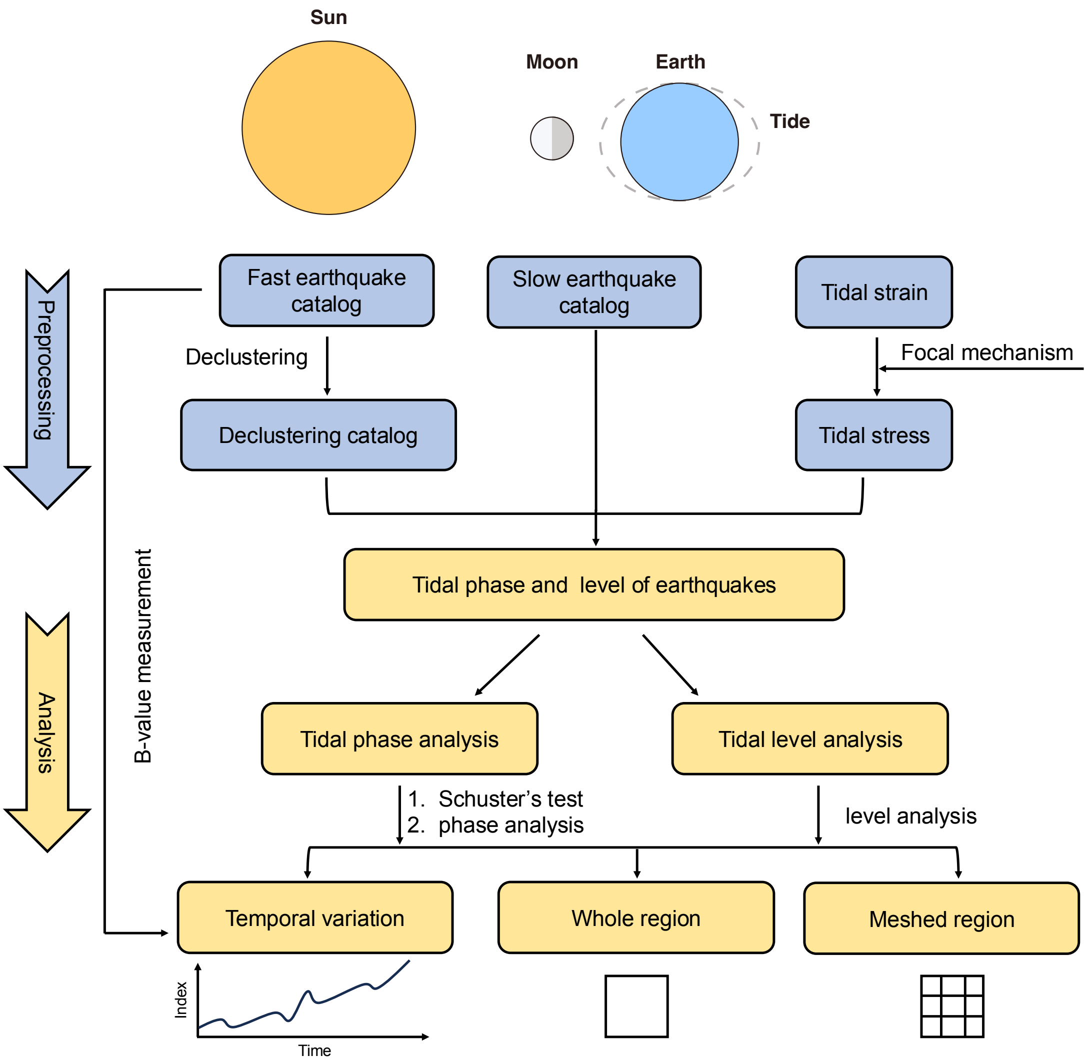

Figure 1. Basic flow of the TiMEpy package.

3. Implementation

3.1 Earthquake selection and declustering

Input earthquake catalog can be either a unified catalog or a regional one. Once the region of interest is defined, simply specify the time range, central point, and filtering criteria to rapidly preprocess the catalog. Our program supports various selection shapes—including squares, rectangles, and circles—as well as rotation-based filtering operations.

After inputting the earthquake catalog, declustering is a critical step for fast and effective analysis. Earthquake catalogs inherently contain clustered events, such as foreshocks and aftershocks, which are interdependent due to stress transfer mechanisms rather than external triggers like tidal forces. To isolate primary earthquakes driven by external stress perturbations (e.g., tidal stresses), declustering is essential for minimizing statistical biases and ensuring robust correlation analyses. In this study, two declustering methods are applied: the Nearest-Neighbor Algorithm (NNA) (Zaliapin & Ben-Zion, 2013) and the Reasenberg method (Reasenberg, 1985). The NNA identifies clusters by analyzing spatiotemporal proximity and magnitude differences between events, using localized density thresholds to distinguish background seismicity from clustered sequences (see **Text S1** for detail). Meanwhile, the Reasenberg method employs empirical time-space-magnitude windows to probabilistically classify aftershocks based on rupture zone scaling, aftershock duration, and magnitude decay rates. To accommodate diverse research needs, our framework allows users to select either the NNA or the Reasenberg method for earthquake declustering. This flexibility ensures adaptability to varying tectonic settings, catalog resolutions, or study objectives.

To assess the effectiveness of declustering, we provide visualization tools that enable users to evaluate the "cleanliness" of declustered catalogs by comparing them with raw catalogs. For example, these tools analyze cumulative earthquake counts over time to highlight deviations caused by the removal of clustered events (e.g., aftershocks), ensuring that temporal trends reflect background seismicity rather than earthquake clustering. Additionally, spatial-temporal distributions of earthquakes are visualized along longitude or latitude dimensions, allowing users to detect residual clustering patterns or homogenization effects post-declustering (**Figure S1**). By overlaying declustered and raw catalogs in interactive plots, researchers can visually confirm whether high-density zones (e.g., fault segments or aftershock swarms) have been appropriately filtered, while retaining regionally representative earthquake distributions. This visual validation complements quantitative metrics, ensuring robust declustering outcomes for subsequent tidal modulation analyses.

3.2 Strain-to-Stress conversion

The strain-to-stress conversion process begins with preparing 6-component strain tensors (ε_{xx}, ε_{yy}, ε_{zz}, ε_{xy}, ε_{xz}, ε_{yz}) derived from theoretical tidal strain programs such as TidalStrain2 (Hirose et al., 2019) or SPOTL (Agnew, 2012). In this package, the initial coordinate system follows the GOTIC2 convention, where east, north, and upward are defined as the positive directions of the *x*-, *y*-, and *z*-axes, respectively (**Figure 2a**). To align the strain tensor with an assumed fault geometry, two sequential coordinate rotations are applied:

First Rotation: Transform the original GOTIC2 coordinates (*x*,*y*,*z*) to an intermediate system (x',y',z'), where x' points north, y' points east, and z' points downward, as defined in Aki and Richards (2002). The rotation matrix $A1$ for this transformation is:

$$\boldsymbol{A_1} = \begin{pmatrix} 0 & 1 & 0 \\ 1 & 0 & 0 \\ 0 & 0 & -1 \end{pmatrix} \tag{1}$$

Second Rotation: Transform the intermediate system (x',y',z') to the fault-oriented system (x'', y'', z''), where x'' aligns with the slip direction, y'' is perpendicular to the fault plane (positive fault-normal direction), and z'' is orthogonal to both (z''=x''×y''). The rotation matrix $A2$, parameterized by the fault strike (ϕ_s), dip angle (δ), and rake (λ), is:

$$\boldsymbol{A_2} = \begin{pmatrix} cos\lambda \cos\phi_s + cos\delta sin\lambda sin\phi_s & cos\lambda\ sin\phi_s - cos\delta\ sin\lambda\ cos\phi_s & -sin\lambda sin\delta \\ -\sin\delta\ sin\phi_s & sin\delta cos\phi_s & -cos\delta \\ * & * & * \end{pmatrix} \tag{2}$$

The third row of Equation 2 (omitted here for brevity) is derived as the cross product of the first two rows.

The total rotation matrix $\boldsymbol{A} = \boldsymbol{A_2 A_1}$ transforms the strain tensor E from the original coordinate system to the fault-oriented system via $E'' = AEA^T$. Using the six independent strain components (ε_{xx}, ε_{yy}, ε_{zz}, ε_{xy}, ε_{xz}, ε_{yz}), the volumetric strain $\varepsilon_{vol} = \varepsilon_{xx} + \varepsilon_{yy} + \varepsilon_{zz}$ (coordinate-invariant) is calculated. The tidal stress perturbations on the fault—shear stress (τ) and normal stress (σ), and Coulomb failure stress (τ_{cfs})—are then computed as:

$$\tau = 2\mu_L \varepsilon_{x''y''} \tag{3}$$

$$\sigma = \lambda_L \varepsilon_{vol} + 2\mu_L \varepsilon_{y''y''} \tag{4}$$

$$\tau_{cfs} = \tau + \mu\sigma \tag{5}$$

Where $\lambda_L = \rho({V_p}^2 - 2{V_s}^2)$ and $\mu_L = \rho {V_s}^2$are Lamé parameters derived from crustal density (ρ), P-wave velocity (V_p), and S-wave velocity (V_s), and μ is the apparent friction coefficient. This framework enables precise evaluation of tidal stress contributions to fault activation, critical for analyzing tidal-earthquake correlations.

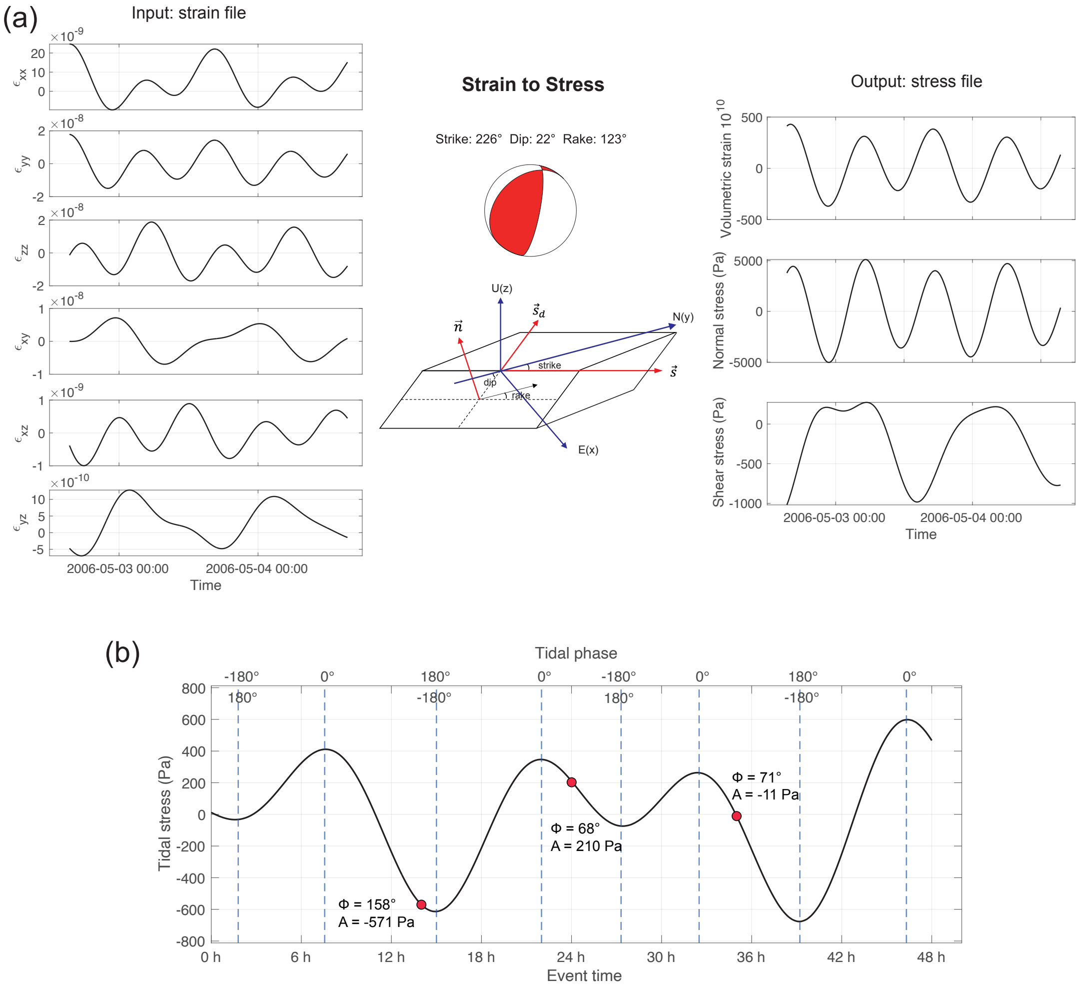

Figure 2. (a) The process of converting the input strain time series (left panels) into volumetric, normal, and shear stress components (right panels) using the specified fault-plane parameters. (b) Estimation of tidal phase angles (φ) and tidal stress (A) at earthquake occurrence times (circle) from the temporal variations in tidal stress.

3.3 Earthquake occurrence in relation to tidal phase and level

After obtaining the tidal stress, we determine the tidal phase angle and level. The local tidal minima before and after each event are assigned phase angles of -180° and +180°, respectively, while the maximum tidal value between these two minima is set to 0° (Cochran et al., 2004). The tidal phase angle and tidal level A at the time of the earthquake are estimated using linear interpolation within the time intervals from -180° to 0° or from 0° to +180° (**Figure 2b**). Here, tidal level A is defined as the strain or stress value, with a positive or negative sign relative to the zero line.

3.4 Tidal modulation by tidal phase

After obtaining the tidal phase and tidal level, the next step is to analyze tidal modulation. One widely used approach for this purpose is Schuster's test (Schuster, 1897), which evaluates whether earthquake occurrences are non-uniformly distributed with respect to the tidal phase (**Figure 3a**). The test statistic is calculated as follows:

$$D^2 = \left(\sum_{i=1}^{N} cos\varphi_i\right)^2 + \left(\sum_{i=1}^{N} sin\varphi_i\right)^2 \tag{6}$$

The p-value, which determines the statistical significance of the result, is calculated as:

$$p = \exp\left(-\frac{D^2}{N}\right) \tag{7}$$

Where N is the total number of earthquakes, φ_i is tidal phase angle. A smaller p-value indicates stronger evidence against the null hypothesis, which assumes that earthquakes occur randomly with respect to the tidal phase. If the test yields a statistically significant result (typically, $p < 0.05$, as suggested by Tanaka et al. (2002)), it suggests that tidal modulation may influence earthquake occurrence. A detailed description of the physical process underlying Schuter's test can be found in **Text S2**.

To complement traditional statistical tests (e.g., Schuster's test), we introduce a physics-driven framework to quantify tidal modulation of seismicity (Beaucé et al., 2023; Beeler & Lockner, 2003; Lockner & Beeler, 1999; Lu, Xue, et al., 2025). The methodology proceeds as follows:

For each earthquake in the declustered catalog, the tidal phase angle (φ) is calculated using the interpolation scheme. The resulting collection of phase angles forms the observed phase distribution, $P_{obs}(\varphi)$, which captures the empirical relationship between tidal stress states and earthquake occurrence (**Figure 3b**). To account for tidal stress heterogeneity over time, we generate synthetic "background" seismicity by uniformly sampling timestamps at 1-hour intervals within the same temporal range as the observational catalog. For each synthetic timestamp, the corresponding tidal phase angle is computed, yielding a reference distribution $P_{ref}(\varphi)$. This distribution reflects the expected seismicity rate if earthquakes are independent of tidal stresses, weighted by the time duration spent in each phase bin.

The modulation is then quantified via the seismicity density ratio:

$$R_\Phi(\varphi) = \frac{P_{obs}(\varphi)}{P_{ref}(\varphi)} \tag{8}$$

computed for each phase bin—where ρ_{obs} and ρ_{ref} denote the normalized earthquake counts per unit time in P_{obs} and P_{ref}, respectively (**Figure 3c**).

To characterize the distribution of R_Φ, we model it using a periodic function:

$$R_\Phi(\varphi) = Pcos(\varphi - \varphi_0) \tag{9}$$

In this expression, P, known as the tidal phase amplitude, quantifies the strength of tidal modulation, while φ_0, the tidal phase shift, indicates the angular position at which seismicity peaks. This formulation captures the cyclical nature of tidal influences on seismicity, allowing for a direct estimation of modulation amplitude and phase alignment with respect to tidal stress variations. By fitting this function to the observed $R_\Phi(\varphi)$ ratio distribution, we can assess the extent to which earthquake occurrence is modulated by tidal forces and determine the phase shift at which seismic activity reaches its maximum. The bigger P, the stronger the tidal modulation is.

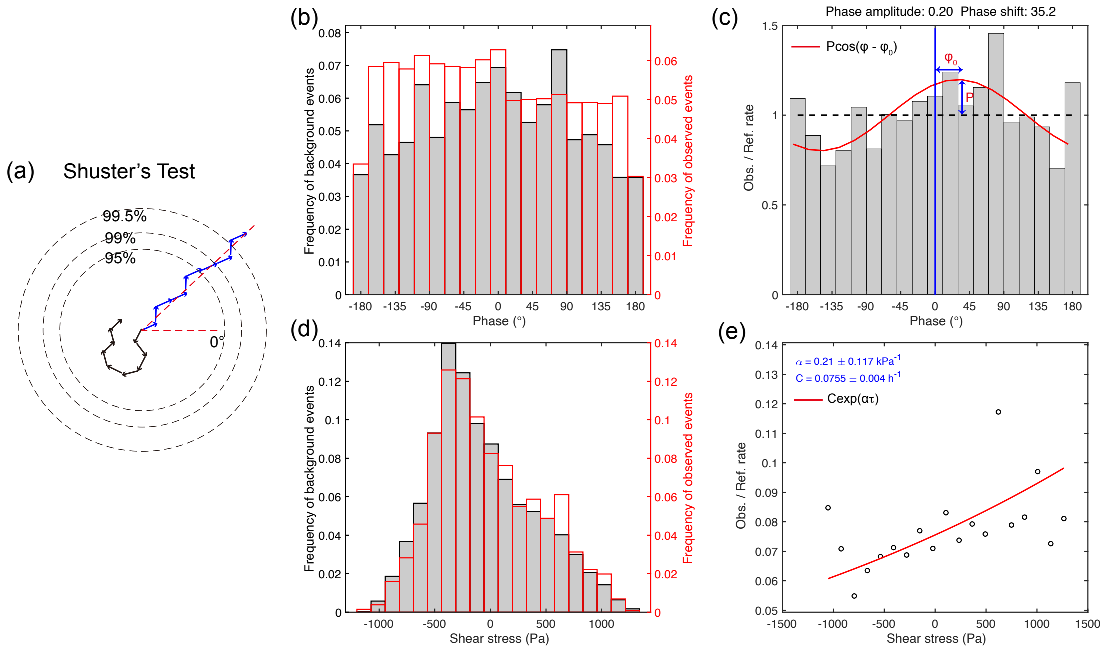

Figure 3. Different methods for detecting tidal modulation. (a) Shuster's test. (b, c) Tidal modulation based on tidal phase information. In (b), the gray bars represent the reference (background) distribution of tidal phase angles sampled hourly, while the red-outlined bars show the actual observed tidal phase angle distribution. In (c), the ratio of observed to reference tidal phase angles is plotted, with the red curve indicating a fitted sinusoidal function. (d, e) Tidal modulation analysis based on tidal level. In (d), the gray bars represent the reference (background) distribution of tidal stress (sampled hourly), whereas the red-outlined bars depict the observed tidal stress distribution. In (e), the black circles show the ratio of observed events to the background distribution, and the red curve represents the event occurrence rate calculated using MLE estimates of two parameters are also shown.

3.5 Tidal modulation by tidal level

To evaluate whether the likelihood of an earthquake increases with rising tidal level, we adopted the following method (Houston, 2015; Ide et al., 2015; Lu, Ide, et al., 2025;

Yabe et al., 2015). First, tidal levels were uniformly sampled at hourly intervals to generate what we refer to as the theoretical tidal level distribution (P_{ref}). Next, this theoretical distribution was compared to the distribution of earthquake occurrences (P_{obs}). As shown in **Figure 3d**, the red area represents the duration spent at each tidal level, while the gray area corresponds to the observed earthquake events. Dividing the red area by the gray area yields the ratio:

$$R_{\Sigma}(\tau) = \frac{P_{obs}(\tau)}{P_{ref}(\tau)} \tag{10}$$

We then fit this ratio with an exponential function:

$$R_{\Sigma}(\tau) = C\exp\left(\alpha\tau\right) \tag{11}$$

where R is the earthquake rate, C is a reference earthquake rate when tidal stress is zero, τ is the tidal stress, and α is the tidal sensitivity. This exponential relationship between tidal stress and earthquake occurrence has been supported by observational studies (Beeler & Lockner, 2003; Houston, 2015; Ide et al., 2015) as well as by theoretical analyses using a simple spring-block system with rate-and-state friction (RSF) (Ader et al., 2012). We use the maximum likelihood method to estimate the parameter α and C. The uncertainty is quantified using the Hessian matrix of the negative log-likelihood function at its optimum. The inverse of the Hessian gives the covariance matrix, and the square roots of its diagonal elements provide the standard errors for α and C. These errors allow us to approximate 95% confidence intervals, typically as twice the standard error.

3.6 B-value measurement

To complement our tidal modulation analysis, we incorporate the earthquake b-value, a parameter derived from the Gutenberg-Richter relationship that quantifies the relative occurrence of small and large events, to further evaluate how tidal stresses may influence stress heterogeneity and seismicity. We employ a novel b-value estimator called "b-positive," which is based solely on the positive differences in magnitude between successive earthquakes (van der Elst, 2021). The standard deviation of the estimated b-value is computed using the bootstrap method (Efron, 1982).

3.7 Package features

Python is an ideal choice for developing projects like TiMEpy thanks to its ease of use and readability, along with a vast ecosystem of libraries (e.g., NumPy, Pandas, SciPy, Matplotlib). TiMEpy is a novel framework for tidal modulation built on the Python workflow and closely integrated with the seismological ecosystem, including ObsPy (Beyreuther et al., 2010). In TiMEpy, each process is executed with exceptional clarity, and individual steps can be seamlessly linked to other research tasks, such as earthquake declustering and b-value estimation. The adjustable parameters are stored in input_params.py. The schematic (**Figure 4**) illustrates an example workflow. The main functions included in the TiMEpy package are:

1. Earthquake declustering.
2. Associating earthquake timing information with tidal stress.
3. Tidal modulation analysis based on level and phase.
4. B-value estimation.

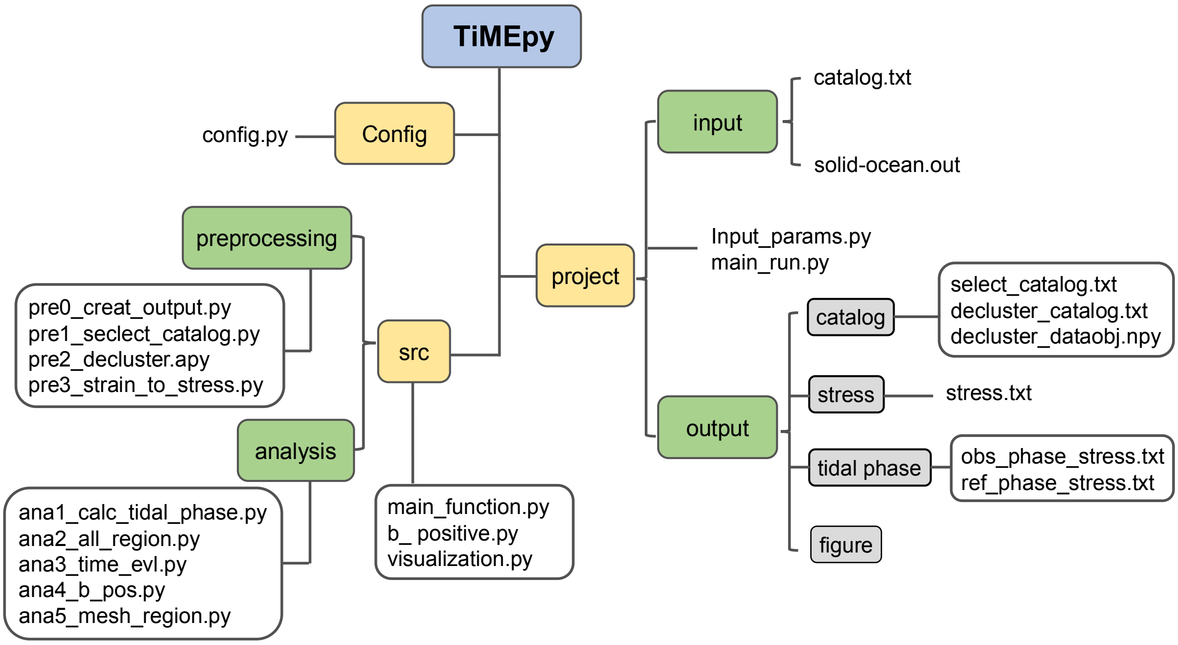

Figure 4. Schematic diagram illustrating the usage of the TiMEpy package. The yellow box denotes the first directory of the package, and the green box denotes the second directory. The .py files in the Config folder generate images and store file names, while the Src folder contains TiMEpy's core functions. The Project folder can be renamed to match different study areas by simply updating the Input_params file.

4. Applications

4.1 2019 M7.1 Ridgecrest, California Earthquake

A nearly 20-year hiatus in major seismic activity in southern California ended on July 4, 2019, when a sequence of intersecting earthquakes occurred near Ridgecrest. Among these events was the significant Mw 7.1 Ridgecrest earthquake (Ross, Idini, et al., 2019;

Yue et al., 2021). To shed light on the region's seismic behavior leading up to this event, Beaucé et al. (2023) analyzed 10 years of continuous seismic waveforms preceding the 2019 Ridgecrest, CA earthquake sequence. By employing earthquake detection and location methods based on machine learning and template matching, they detected 191,569 earthquakes (**Figure 5a**). Their enhanced catalog revealed that seismicity became strongly modulated by the tides approximately two years before the mainshock. Notably, instead of declustering, they used a stacking method to mitigate the clustering effect. Therefore, applying our program to analyze the same catalog provides a robust test of its performance.

We used an updated version of the earthquake catalog developed by Beaucé et al. (2023), although the updated version contains fewer events. The fault region of interest we selected is essentially consistent with that used by Beaucé et al. (2023). First, we applied the NNA for declustering the earthquake catalog. The nearly linear trend in the cumulative number of events after declustering indicates that this procedure was highly effective. Next, we computed the strain components using TidalStrain2. Based on the mainshock's focal mechanism (strike = 321°, dip = 81°, rake = 180°) (**Table S1**), we projected the tidal stresses onto the fault plane. The normal and shear components were then combined to calculate the coulomb stress according to Equation (5) with a friction coefficient μ=0.6. **Figure 5d** illustrates the relationship between the declustered earthquake catalog and the tidal Coulomb stress.

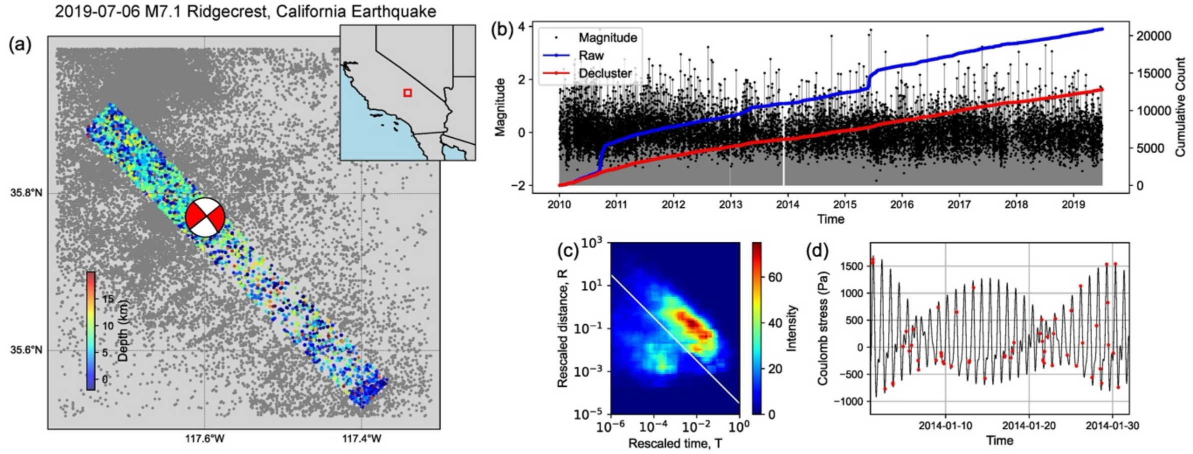

Figure 5. (a) Spatial distribution of the enhanced catalog from Beaucé et al. (2023), highlighting a 5 km-wide region of interest containing 20,848 earthquakes. (b) The blue line shows the cumulative number of earthquakes within the box over time, while the red line indicates the cumulative count after declustering. The background points represent the Magnitude–Time (M–T) plot. (c) Joint distribution of rescaled time (T) and space (R) components for the nearest-neighbor proximity. (d) One month of tidal Coulomb stress on a fault optimally oriented in the regional stress field, with red dots

marking the times of earthquake occurrences.

We computed $R_{\phi}(\varphi)$ and $R_{\Sigma}(\tau)$ in overlapping 3.4-year windows with 3-month steps, , with these parameters adopted from Beaucé et al. (2023) (**Table S2**). Each window comprises at least about 3,700 events (**Figure S2**). Tidal phase analysis reveals that after 2018, the tidal phase shift angle gradually converges toward 0°, while the amplitude of tidal phase steadily increases (**Figure 6a** and **6b**). Additionally, the tidal sensitivity results also indicate enhanced tidal modulation (**Figure 6d**). We selected a significant point to provide detailed information, as shown in **Figure 6c** and **6e**. These findings are consistent with those of Beaucé et al. (2023), demonstrating a strong tidal modulation effect starting about 1.5 years before the mainshock. Additionally, the b-value begins to decrease prior to the mainshock (**Figure 6e**), which aligns with the findings reported by Nanjo (2020)

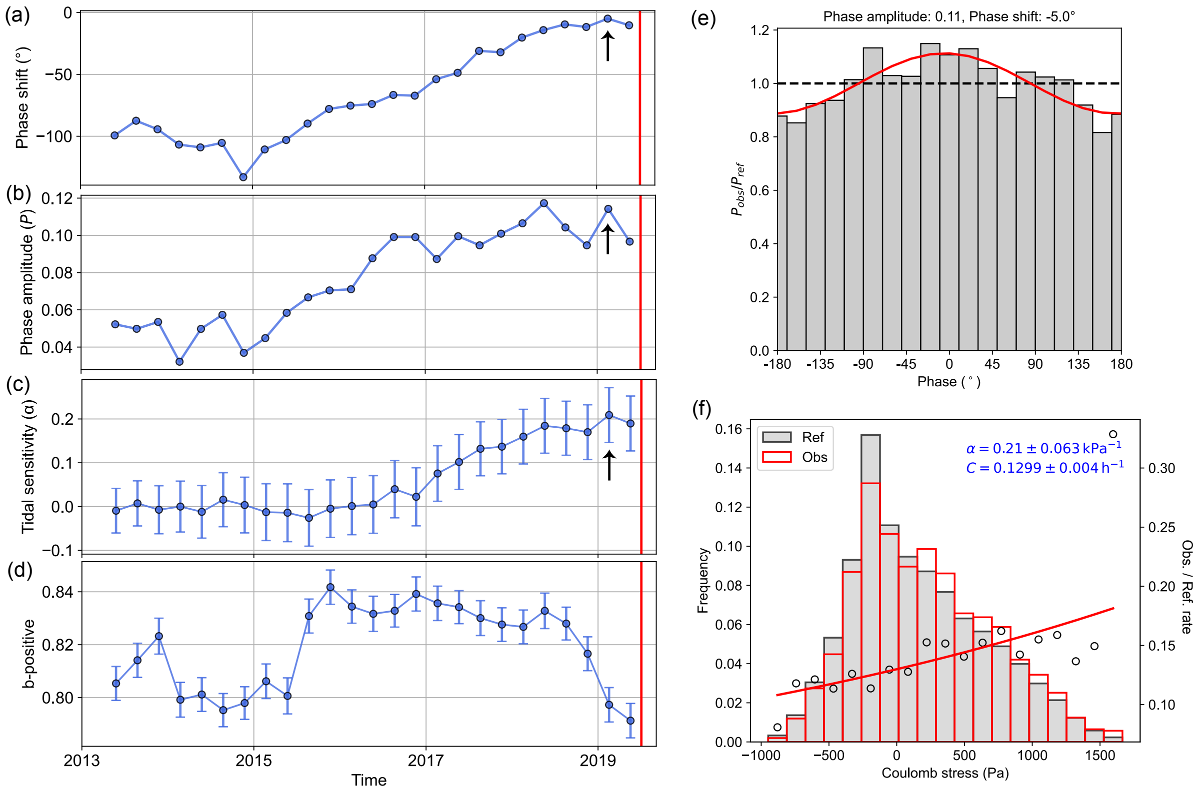

Figure 6. Analysis of the tidal modulation of seismicity in terms of phase and amplitude. (a) Temporal variation of phase shift. The 0° line corresponds to the maximum Coulomb stress, while −90° represents the maximum coulomb stress rate. (b) Temporal variation of amplitude (P) of distribution of phase shift. (c) Temporal variation of tidal sensitivity derived from tidal amplitude. (d) Temporal variation of b-positive. In (a)-(d), each dot is at the end of the window over which the measurement was made. (e) Cosine fits, $\alpha\cos(\varphi - \varphi_0)$, where red dots indicate intervals showing tidal phase modulation. (f) Histogram of hourly levels of shear stress (gray) and the number of events (red) for the

study period. Number of events per hour for each bin in linear (red) for shear stress. The lines calculated using MLE estimates of two parameters are also shown.

4.2 2012-2022 Tectonic tremors in Taiwan

Using continuous seismic data from multiple recently available stations in Taiwan, Ide and Chen (2024) applied the envelope correlation method to detect approximately 7,000 tremor events between 2012 and 2022. This new tremor catalog serves as an excellent example for testing the reliability of TiMEpy. We selected a prominent tremor cluster located beneath the Central Mountain Range, comprising 4,666 tremors—the largest and most significant tremor cluster identified in Taiwan (Ide & Chen, 2024) (**Figure 7a**).. Unlike typical earthquakes, tremors occur in a manner that essentially lacks clustering effects, thereby eliminating the need for declustering (**Figure 7b**). The focal mechanism we adopted is derived from Ide et al. (2015) and represents a low-angle reverse faulting process (strike = 54°, dip = 13°, rake = 120°), which has been substantiated by evidence of low-angle reverse slip on the fault plane in this region (Ide & Chen, 2024).

Figure 7a displays a comparison between the timing of the 4,666 tremors and the tidal shear stress. It clearly demonstrates that tremors occur when the tidal shear stress is positive, as highlighted by the red dots. The relationship between tidal stress and tremor rate in this cluster reveals that, as shear stress increases, the tremor rate exhibits a nonlinear increase, with a tidal sensitivity reaching as high as 1.49 (**Figure 7b**). Compared to regions such as Nankai and the Cascade (Yabe et al., 2015), the tidal sensitivity in this case is significantly higher. Furthermore, compared with Ide et al. (2015), the tidal sensitivity of 2.1 derived from the 2007–2012 tremor catalog is lower, suggesting that tremor's sensitivity to tidal forcing may have changed over time, reflecting shifts in the region's tectonic setting. Additionally, the tidal phase angle distribution is nearly 0°, and the amplitude of the tidal phase is exceptionally high (**Figure 7c**).

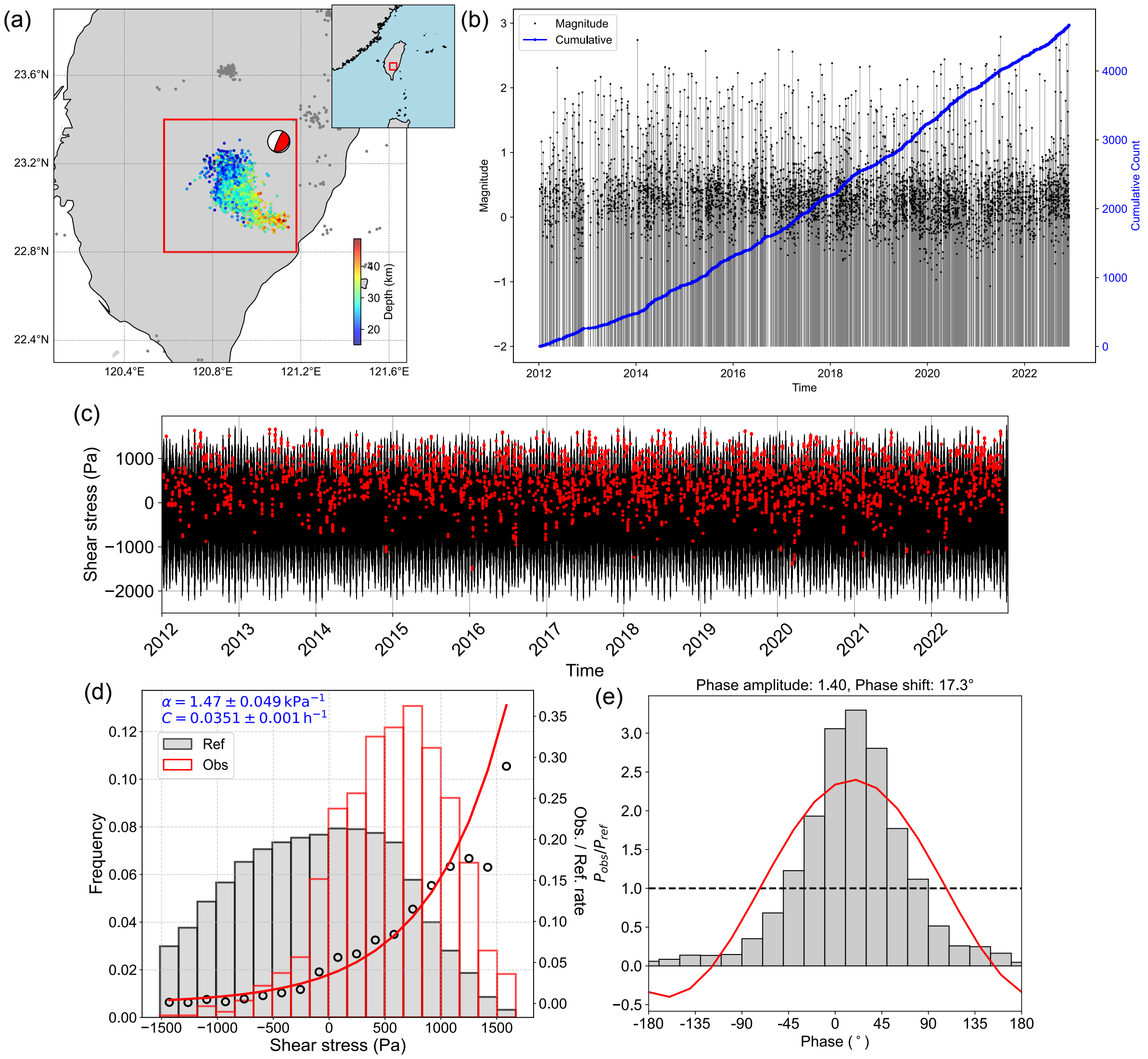

Figure 9. (a) Map view of tremor distribution, with color gradients indicating tremor depths. (b) M–T plot and cumulative number of tremors. (c) Tidal shear stress, with red dots marking the occurrence times of tremors. (d) Same as Figure 6f. (e) Same as Figure 6e.

5. Discussion and conclusions

Exploring the correlation between seismicity and tidal stress remains a challenging endeavor due to the inherent complexity of the analytical methods involved (Zhao et al., 2025). Unlike straightforward earthquake detection, integrating tidal influences into seismic analysis is complicated by the use of diverse methodologies for assessing seismic activity, calculating tidal stresses, and performing tidal modulation analysis. These variations have sparked considerable debate in the pervious studies. For example, Tanaka (2012) reported evidence of tidal triggering preceding the 2011 Tohoku-Oki earthquake, whereas Wang and Shearer (2015) found no clear triggering signal before the event. Nonetheless, in regions where the correlation between seismicity and tidal stress is pronounced, differences in analytical methods and parameter selections do not seem to lead to significant discrepancies. When utilizing an enhanced earthquake catalog based on Beaucé et al. (2023) and applying our tidal modulation detection approach, clear tidal modulation signals were observed as early as two years prior to an earthquake, underscoring the robustness of this correlation in such areas.

In order to make tidal modulation analysis more accessible, we designed a Python package called TiMEpy for detecting tidal modulation in both fast and slow earthquakes. We hope that by open-sourcing the package, seismologists will more easily incorporate tidal modulation methods into their research. Integrating TiMEpy within the Python ecosystem streamlines package updates based on user feedback and enhances flexibility and creativity for researchers. By leveraging widely used libraries for statistical computation, array processing, interpolation, map projection, and tabular data management, TiMEpy delivers robust and reliable performance. Its deliberately modular design allows users to modify specific components to suit their scientific objectives. For example, in earthquake declustering, researchers may choose to apply certain algorithms according to their focus or even omit this step for studies centered on slow earthquakes. The package also supports alternative declustering approaches, including ETAS (Zhuang et al., 2002), custom methods to mitigate clustering effects (Beaucé et al., 2023; Wang & Shearer, 2015), and the use of synthetic catalogs to test and ensure consistency in modulation (Delorey et al., 2017). In addition, several modules, such as the b-value measurement module, can operate independently, further highlighting the tool's versatility and extensibility.

A key focus for future research is to leverage the correlation between seismicity and tidal stress to derive earthquake physical parameters (e.g. background normal stress). Currently, the timing of earthquakes relative to earthquakes and tidal triggering stress is consistent with certain aspects of the tidal load-triggered earthquake model proposed by Beeler and Lockner (2003). However, some discrepancies remain. For example, the recurrence time is shorter than the calculated earthquake nucleation time, the failure time appears to be related to the stress rate, and the effects of fault creep are neglected. These issues constrain the broader applicability of the Beeler and Lockner (2003) model. We hope that by widely adopting this package to detect representative regions, researchers will be able to reliably derive parameters relevant to earthquake physical processes.

In summary, the development of TiMEpy, a user-friendly tidal modulation analysis package, provides a robust and versatile tool for investigating tidal influences on seismicity. By leveraging widely used Python libraries and a modular design, TiMEpy not only streamlines the integration of tidal modulation methods into seismological research but also supports flexible customization for diverse scientific objectives. We anticipate that the widespread adoption of TiMEpy will significantly advance our understanding of earthquake physical parameters and contribute to the refinement of theoretical frameworks.

Data and Resources

The software described in this study is documented and publicly available in the repository at https://github.com/Weifan-Lu/TiMEpy. The TidalStrain.2 can be accessed at https://www.mri-jma.go.jp/Dep/sei/fhirose/research/en.TidalStrain.html. The Ridgecrest earthquake catalog is available on the Zenodo platform at https://zenodo.org/records/8393318. The 2012-2022 tectonic tremor catalog is available at http://www-solid.eps.s.u-tokyo.ac.jp/~sloweq/?page=map.

Acknowledgements

We thank Lian Xue, Satoshi Ide, Han Yue and Zeyan Zhao for their helpful discussion.

Declaration of Competing Interests

The authors acknowledge that there are no conflicts of interest recorded.

References:

Ader, T. J., Ampuero, J.-P., & Avouac, J.-P. (2012). The role of velocity-neutral creep on the modulation of tectonic tremor activity by periodic loading. *Geophysical Research Letters*, *39*(16). https://doi.org/10.1029/2012GL052326

Agnew, D. C. (2012). SPOTL: Some programs for ocean-tide loading (Version 3.3.0.2). *[Software]*. https://doi.org/https://igppweb.ucsd.edu/~agnew/Spotl/spotlmain.html

Aki, K., & Richards, P. G. (2002). Quantitative Seismology. *Quantitative Seismology*.

Beaucé, E., Poli, P., Waldhauser, F., Holtzman, B., & Scholz, C. (2023). Enhanced Tidal Sensitivity of Seismicity Before the 2019 Magnitude 7.1 Ridgecrest, California Earthquake. *Geophysical Research Letters*, *50*(14), e2023GL104375. https://doi.org/10.1029/2023GL104375

Beeler, N. M., & Lockner, D. A. (2003). Why earthquakes correlate weakly with the solid Earth tides: Effects of periodic stress on the rate and probability of earthquake occurrence. *Journal of Geophysical Research: Solid Earth*, *108*(B8). https://doi.org/10.1029/2001JB001518

Beeler, N. M., Thomas, A., Bürgmann, R., & Shelly, D. (2013). Inferring fault rheology from low‐frequency earthquakes on the San Andreas. *Journal of Geophysical Research: Solid Earth*, *118*(11), 5976-5990.

Beyreuther, M., Barsch, R., Krischer, L., Megies, T., Behr, Y., & Wassermann, J. (2010). ObsPy: A Python Toolbox for Seismology. *Seismological Research Letters*, *81*(3), 530-533. https://doi.org/10.1785/gssrl.81.3.530

Cochran, E. S., Vidale, J. E., & Tanaka, S. (2004). Earth Tides Can Trigger Shallow Thrust Fault Earthquakes. *Science*, *306*(5699), 1164-1166. https://doi.org/doi:10.1126/science.1103961

Cotton, L. A. (1922). Earthquake frequency, with special reference to tidal stresses in the lithosphere. *Bulletin of the Seismological Society of America*, *12*(2-3), 47-198. https://doi.org/10.1785/bssa0120020047

Delorey, A. A., van der Elst, N. J., & Johnson, P. A. (2017). Tidal triggering of earthquakes suggests poroelastic behavior on the San Andreas Fault. *Earth and Planetary Science Letters*, *460*, 164-170. https://doi.org/10.1016/j.epsl.2016.12.014

Efron, B. (1982). *The jackknife, the bootstrap and other resampling plans*. SIAM.

Guo, H., Ross, Z., Wilding, J., & Avouac, J.-P. (2026). In-situ fault properties and earthquake nucleation revealed by tidal modulation of seismicity.

Heaton, T. H. (1982). Tidal triggering of earthquakes. *Bulletin of the Seismological Society of America*, *72*(6A), 2181-2200.

Hirose, F., Maeda, K., & Kamigaichi, O. (2019). Tidal Forcing of Interplate Earthquakes Along the Tonga-Kermadec Trench. *Journal of Geophysical Research: Solid Earth*, *124*(10), 10498-10521. https://doi.org/10.1029/2019JB018088

Houston, H. (2015). Low friction and fault weakening revealed by rising sensitivity of tremor to tidal stress. *Nature Geoscience*, *8*(5), 409-415. https://doi.org/10.1038/ngeo2419

Ide, S., & Chen, K. H. (2024). Spatiotemporal Characteristics of Tectonic Tremors in the Collisional Orogen of Taiwan. *Geophysical Research Letters*, *51*(4), e2023GL106759. https://doi.org/10.1029/2023GL106759

Ide, S., Yabe, S., Tai, H.-J., & Chen, K. H. (2015). Thrust-type focal mechanisms of tectonic tremors in Taiwan: Evidence of subduction. *Geophysical Research Letters*, *42*(9), 3248-3256. https://doi.org/10.1002/2015GL063794

Lockner, D. A., & Beeler, N. M. (1999). Premonitory slip and tidal triggering of earthquakes. *Journal of Geophysical Research: Solid Earth*, *104*(B9), 20133-20151. https://doi.org/10.1029/1999jb900205

Lu, W., & Ide, S. (2026). Spatiotemporal Characteristics of Tectonic Tremors in California. *Geophysical Research Letters*, *53*(4), e2025GL120742. https://doi.org/10.1029/2025GL120742

Lu, W., Ide, S., & Yue, H. (2025). Small-scale stress heterogeneity inferred many anti-repeating earthquakes in Sierra Valley, Nevada. *Earth, Planets and Space*, *77*(1), 142. https://doi.org/10.1186/s40623-025-02273-y

Lu, W., Xue, L., Yue, H., Zhuang, J., & Zhao, L. (2025). Exploring Tidal Modulation of Seismicity in Southern California. *Journal of Geophysical Research: Solid Earth*, *130*(12), e2025JB032249. https://doi.org/10.1029/2025JB032249

Nanjo, K. Z. (2020). Were changes in stress state responsible for the 2019 Ridgecrest, California, earthquakes? *Nature Communications*, *11*(1), 3082. https://doi.org/10.1038/s41467-020-16867-5

Obara, K. (2002). Nonvolcanic deep tremor associated with subduction in southwest Japan. *Science*, *296*(5573), 1679-1681.

Reasenberg, P. (1985). Second-order moment of central California seismicity, 1969-1982. *Journal of Geophysical Research: Solid Earth*, *90*(B7), 5479-5495. https://doi.org/10.1029/JB090iB07p05479

Ross, Z. E., Idini, B., Jia, Z., Stephenson, O. L., Zhong, M., Wang, X., Zhan, Z., Simons, M., Fielding, E. J., Yun, S.-H., Hauksson, E., Moore, A. W., Liu, Z., & Jung, J. (2019). Hierarchical interlocked orthogonal faulting in the 2019 Ridgecrest earthquake sequence. *Science*, *366*(6463), 346-351. https://doi.org/doi:10.1126/science.aaz0109

Ross, Z. E., Trugman, D. T., Hauksson, E., & Shearer, P. M. (2019). Searching for hidden earthquakes in Southern California. *Science. [Dataset]. 364*(6442), 767-771.

Schuster, A. (1897). On lunar and solar periodicities of earthquakes. *Proceedings of the Royal Society of London*, *61*(369-377), 455-465. https://doi.org/doi:10.1098/rspl.1897.0060

Shelly, D. R., Beroza, G. C., & Ide, S. (2007). Non-volcanic tremor and low-frequency earthquake swarms. *Nature*, *446*(7133), 305-307.

Shelly, D. R., Thomas, A. M., Materna, K. Z., & Skoumal, R. J. (2026). Low-frequency earthquakes track the motion of a captured slab fragment. *Science*, *391*(6782), 294-299. https://doi.org/doi:10.1126/science.aeb2407

Shudde, R., & Barr, D. (1977). An analysis of earthquake frequency data. *Bulletin of the Seismological Society of America*, *67*(5), 1379-1386.

Sirorattanakul, K., & Avouac, J.-P. (2026). Seismic rhythms: Earthquake response to tectonic, hydrological, and tidal forcing in California. *Science Advances*, *12*(13), eadz5711. https://doi.org/doi:10.1126/sciadv.adz5711

Tanaka, S. (2012). Tidal triggering of earthquakes prior to the 2011 Tohoku-Oki earthquake (M 9.1). *Geophysical Research Letters*, *39*(7). https://doi.org/10.1029/2012GL051179

Tanaka, S., Ohtake, M., & Sato, H. (2002). Spatio-temporal variation of the tidal triggering effect on earthquake occurrence associated with the 1982 South Tonga earthquake of Mw 7.5. *Geophysical Research Letters*, *29*(16), 3-1-3-4. https://doi.org/10.1029/2002gl015386

Thomas, A., Bürgmann, R., Shelly, D. R., Beeler, N. M., & Rudolph, M. (2012). Tidal triggering of low frequency earthquakes near Parkfield, California: Implications for fault mechanics within the brittle‐ductile transition. *Journal of Geophysical Research: Solid Earth*, *117*(B5).

van der Elst, N. J. (2021). B-Positive: A Robust Estimator of Aftershock Magnitude Distribution in Transiently Incomplete Catalogs. *Journal of Geophysical Research: Solid Earth*, *126*(2), e2020JB021027. https://doi.org/10.1029/2020JB021027

Vidale, J. E., Agnew, D. C., Johnston, M. J. S., & Oppenheimer, D. H. (1998). Absence of earthquake correlation with Earth tides: An indication of high preseismic fault stress rate. *Journal of Geophysical Research: Solid Earth*, *103*(B10), 24567-24572. https://doi.org/10.1029/98jb00594

Wang, W., & Shearer, P. M. (2015). No clear evidence for localized tidal periodicities in earthquakes in the central Japan region [Article]. *Journal of Geophysical Research: Solid Earth*, *120*(9), 6317-6328. https://doi.org/10.1002/2015JB011937

Xue, L., Bürgmann, R., Zhao, Z., Beeler, N. M., Heimisson, E. R., & Shelly, D. R. (2025). Probing lower-crustal fault properties with frequency-dependent tidal tremor triggering. *Earth and Planetary Science Letters*, *666*, 119480. https://doi.org/10.1016/j.epsl.2025.119480

Yabe, S., Tanaka, Y., Houston, H., & Ide, S. (2015). Tidal sensitivity of tectonic tremors in Nankai and Cascadia subduction zones. *Journal of Geophysical Research: Solid Earth*, *120*(11), 7587-7605. https://doi.org/10.1002/2015JB012250

Yue, H., Sun, J., Wang, M., Shen, Z., Li, M., Xue, L., Lu, W., Zhou, Y., Ren, C., & Lay, T. (2021). The 2019 Ridgecrest, California earthquake sequence: Evolution of seismic and aseismic slip on an orthogonal fault system. *Earth and Planetary Science Letters*, *570*, 117066. https://doi.org/doi.org/10.1016/j.epsl.2021.117066

Zaliapin, I., & Ben-Zion, Y. (2013). Earthquake clusters in southern California I: Identification and stability. *Journal of Geophysical Research: Solid Earth*, *118*(6), 2847-2864. https://doi.org/10.1002/jgrb.50179

Zhao, Z., Xue, L., Bürgmann, R., Heimisson, E. R., Lu, W., & Yue, H. (2025). Tidal and hydrological seismicity modulations reveal pore fluid diffusion during earthquake nucleation. *Science Advances*, *11*(49), eady6350. https://doi.org/doi:10.1126/sciadv.ady6350

Zhuang, J., Ogata, Y., & Vere-Jones, D. (2002). Stochastic Declustering of Space-Time Earthquake Occurrences. *Journal of the American Statistical Association*, *97*(458), 369-380. https://doi.org/10.1198/016214502760046925